Group movement dynamics improves aerobic performance and conserves anaerobic energy in schooling fish

Short title: Energy conservation by schooling fish

Yangfan Zhang[1]*, George V. Lauder[1],

[1]Department of Organismic and Evolutionary Biology, Harvard University, 26 Oxford St, Cambridge, Massachusetts, 02138, USA

*Corresponding author. Email: yangfan_zhang@fas.harvard.edu

Abstract:

Schooling fish move in a viscous fluid environment and are a model system for understanding how group movement dynamics enables energy conservation[1]. But how group movement in the water reduces locomotor cost remains elusive. We measured both aerobic and anaerobic metabolic contributions to energy use in schools of giant danio, and show an energetic reduction per tail beat of up to 126% compared to solitary fish. Fish in schools used a smaller proportion of their aerobic capacity to swim and reduced the anaerobic cost by 2.8 fold, which lowered the total energy expenditure and cost of transport by up to 112% at higher speeds. Fish schools also exhibit a *U*-shaped metabolism–speed curve, with a minimum metabolic cost at 1 body length s^{-1}, the migratory speed of diverse fish species[2,3]. This finding suggests that physical constraints on movement through water may be a key driver for the evolution of active directional schooling behaviour in fishes.

One-Sentence Summary: Fish schools reduce the metabolic cost of swimming by up to 112% and the energy used per tail beat of up to 126% compared to solitary fish.

Main Text: Newton's laws of motion underpin animal locomotion, from fine-scale maneuvers to long-distance migrations[4]. Since fluid drag scales as velocity squared[5], movement at higher speeds places a premium on mechanisms to conserve energy. As speed increases or during migration involving sustained movement over long distances, animals often move in groups: *e.g.,* migratory birds in V-formations[6], cyclists in a peloton[7], elite marathon runners[8] and fish schools[1]. To overcome gravitational or fluid dynamic resistance to forward motion, animals use metabolism to generate energy and sustain movement in the air, on land, and in the water. The total energy cost of locomotion is met by the amount of energy generated by two metabolic energy sources in vertebrates. Energy use at lower speeds is primarily aerobic, while for high-speed movement anaerobic metabolic pathways are activated to supply the additional (largely shorter-term) energy needs[9]. While whole-animal aerobic metabolism is measured by oxygen (O_2) uptake ($\dot{M}O_2$), the non-aerobic O_2 cost (mostly substrate-level phosphorylation) is measured as excess post-exercise O_2 consumption (EPOC)[10]. Both metabolic energy sources provide the total energy expenditure (TEE) required for movement, and the partitioning of aerobic and anaerobic energy contribution changes as the speed of locomotion increases.

In water, a fluid that is 50-times more viscous than air, the need to reduce hydrodynamic drag for energy conservation is even greater than for aerial or terrestrial locomotion. Here, we use fish schooling as a model system to explore how the hydrodynamics of group movement can enable energetic savings compared to locomotion by solitary individuals. Hydrodynamic models, kinematic studies, and experimental robotic analyses of fish schools indicate that the cost of swimming can be reduced when fish swim beside neighbouring fish[11], directly behind or in front of another fish[12], or in-between leading individuals[1] (Fig. S1). But direct measurements of the metabolic cost of locomotion in fish schools compared to solitary individuals are lacking, and thus how fish schooling behaviour could reduce both the aerobic and anaerobic cost of

locomotion is unknown. No previous study has directly measured the energy use of fish schools over speeds that range from low-speed group locomotion to high-speed directional swimming where the anaerobic metabolic cost of locomotion can be substantial.

We hypothesized that schooling dynamics reduces the TEE in fishes exhibiting active directional schooling (Table S1) over a range of speeds compared to the energy used by solitary fish. We predicted that if collective energy expenditure can be minimized, then fish schools should exhibit a *J*-shaped metabolism-speed curve, and that at high speeds schooling dynamics should enable fish to reduce the anaerobic contribution to TEE and maintain swimming speed compared to anaerobic energy use by solitary fish. A reduction in the anaerobic metabolic contribution at high swimming speeds as a result of schooling dynamics also would reduce the recovery time needed to restore the resting metabolic state compared to locomotion by solitary fish. Furthermore, we expected that fish within schools could become more energetically efficient by reducing the amount of energy expended per tail beat.

To evaluate these hypotheses, we directly measured aerobic and anaerobic energy used by schooling fishes over a wide range of swimming speeds (0.3–8.0 body lengths s^{-1}; BL s^{-1}), and then compared the swimming cost to that of solitary fish. We equipped a high-resolution swim-tunnel respirometer with two orthogonal high-speed cameras mounted on the respirometry system. We simultaneously measured $\dot{M}O_2$, the three-dimensional dynamics of fish schools (n=5) and the kinematics of solitary fish (n=5) (Suppl. Material). This enabled us to focus on the energetics and schooling dynamics of a model species, giant danio (*Devario aequipinnatus*), that exhibits active directional group swimming from minimal speed to maximum sustained speeds (equivalent to a Reynolds number range of $6.4 \cdot 10^3$ to $1.8 \cdot 10^5$; Fig. S2), using a critical swimming speed test (U_{crit}).

We discovered that both fish schools and solitary fish have a *U*-shaped metabolism-speed curve over the lower portion of their speed range (0.3–3 BL s^{-1}, Fig. 1A, D). Danio schools have a minimum aerobic cost ($\dot{M}O_{2min}$ = 212.9 mg O_2 kg^{-1} h^{-1}) at 1.25 BL s^{-1}. $\dot{M}O_{2min}$ at this optimal speed (U_{opt}) was *lower* than both the $\dot{M}O_2$ of aggregating behaviours exhibited before U_{crit} test (Table S1, Fig. S3) and for the group at rest in still water $\dot{M}O_2$ (by 54% and 26% respectively) (F = 16.7, $p \leq 0.02$, Fig. 1A,B). Swimming at U_{opt} reduces the energetic cost below that of swimming at either slower or higher speeds. Indeed, the Strouhal number of fish schools decreased from 2.1 at the lowest speed to 0.3 at the energetic minimum U_{opt}, and then increased to 0.4 at the higher U_{crit}. We also characterized the kinematic features that result in elevated $\dot{M}O_2$ at low speeds. Danio swimming in low-speed aggregations had a higher tail beat frequency (f_{TB}) than solitary fish ($F \geq 9.8$, $p \leq 0.002$). However, at U_{opt} and higher speeds when group directional schooling began, fish in schools had a lower f_{TB} ($F \geq 4.6$, $p \leq 0.035$) than solitary fish (Fig. 3B). The angular heading of schooling fish transitioned from omnidirectional to pointing against water flow when speed is above 0.75 BL s^{-1}, and individual fish orient into the flow starting at 0.3 BL s^{-1} (Fig. 3C). Although body angle and turning frequency of solitary fish and schools decreased with speed, schooling fish had a higher turning frequency ($F \geq 15.6$, $p < 0.002$) below 0.75 BL s^{-1} than solitary fish (Fig. 3D,E).

We discovered that, across the entire 0.3–8 BL s^{-1} range, $\dot{M}O_2$-speed curves of fish schools are *J*-shaped (reached 1053.5 mg O_2 kg^{-1} h^{-1} at 8 BL s^{-1}) whereas solitary fish showed an *S*-shaped curve (reaching a plateau of 760.2 mg O_2 kg^{-1} h^{-1} & ~10% CV) in 6–8 BL s^{-1} (Fig. 1C), demonstrating that schooling dynamics results in a 39% higher aerobic performance (F = 30.0, p < 0.001). At high swimming speeds, aerobic limits are reached, and anaerobic metabolism is engaged to permit continued movement[13]. Often vertebrates at higher speeds use more fast twitch fibers which generate high-frequency contractile force in part through anaerobic glycolysis[14, 15].

99 Given that fish schools have a lower f_{TB} than the solitary fish at 8 BL s^{-1} ($F = 15.1$, $p < 0.001$),
100 we predicted that fish schools, compared with solitary fish, use less anaerobic energy to
101 supplement aerobic energy during exercise. Hence, we measured post-exercise O_2 utilization
102 which is used to restore glycolytically-induced metabolic perturbations (EPOC). We discovered
103 that fish schools have a 2.8-fold lower EPOC ($t = 4.5$, $p = 0.0021$), and recover 1.7-times faster
104 than solitary fish (8 vs 14 h; $t = 2.8$, $p = 0.025$; Fig. 1E,F).

105 Physiological studies of exercise metabolism and locomotion suggest that a higher
106 proportional use of aerobic scope during locomotion relates to a larger accumulation of
107 anaerobic end-products[9]. We show that schooling dynamics results in a lower use of aerobic
108 capacity compared to solitary fish over 0.3–8 BL s^{-1}. Collectively, fish schools used a 36% lower
109 proportion of their aerobic scope than solitary fish (Wilcoxon test: $p = 0.0002$, Fig. 1H). Solitary
110 fish used 38% higher proportion of aerobic scope at 4 BL s^{-1} (50% U_{crit} & > 50% aerobic scope
111 onward), and consistently used ~25% higher proportion of their aerobic scope at 6 and 7 BL s^{-1}
112 than fish schools ($F \geq 4.8$, $p \leq 0.03$, Fig. 1G). Fish often engage glycolysis for swimming above
113 50% U_{crit} [16] and ~50% aerobic scope is a commonly observed inflection point of faster anaerobic
114 end-product accumulation[9]. Collectively, reduced aerobic capacity for swimming above 50%
115 U_{crit} in fish schools likely played a key role in reducing the use of glycolysis for high-speed
116 swimming[10,16].

117 To overcome hydrodynamic drag during swimming, both aerobic and anaerobic
118 metabolic pathways simultaneously fuel muscles to generate locomotor thrust. To estimate the
119 relative proportions of aerobic and anaerobic energy contributions at each swimming speed, we
120 modeled EPOC in addition to $\dot{M}O_2$ (> 50% U_{crit} & aerobic scope, Fig. 2A) (Table S2). We also
121 estimated a total O_2 cost during the entire swimming process for each school and individual and
122 calculated total energy expenditure (TEE) [10]. The TEE of fish schools was 62–112% lower than

123 that of the solitary fish between 5–8 BL s^{-1} ($F \geq 7.4$, $p \leq 0.008$; Fig. 2D). TEE of fish schools
124 was only 42–143 % higher than the aerobic metabolic rate at 5–8 BL s^{-1} ($F \geq 3.5$, $p \leq 0.001$) and
125 anaerobic metabolic energy only accounted for 29–58 % of the TEE depending on speed (Fig.
126 2B). In contrast, TEE of solitary fish was 131–465 % higher than the aerobic metabolic rate
127 between 5–8 BL s^{-1} ($F \geq 10.7$, $p \leq 0.001$), where anaerobic energy accounted for 62–81% of the
128 TEE depending on speed (Fig. 2C).

129 Schooling dynamics reduced the total cost (aerobic plus anaerobic) of transport (TCOT)
130 by an average of 43% compared to swimming alone ($F = 6.9$, $p = 0.01$), and most of this energy
131 conservation happens at higher speeds. Schooling dynamics in danio enables an extremely
132 shallow rate of increase in TCOT with speed compared to that of an individual (Fig. 2E). The
133 TCOT of solitary fish increased by 490% (6.5 kJ km^{-1} kg^{-1}) at 8 BL s^{-1}, whereas the schooling
134 TCOT increased by only 200% (3.6 kJ km^{-1} kg^{-1}) at 8 BL s^{-1}. Notably, the TCOT of fish schools
135 at a swim speed of 3 BL s^{-1} (~1.2 kJ km^{-1} kg^{-1}) is less than the TCOT (1.5 kJ km^{-1} kg^{-1}) of
136 jellyfish moving at < 2 BL s^{-1} [17], one of the most energetically efficient low-speed swimmers (*4*).

137 To answer the question of how schooling dynamics reduces TEE, we combine video
138 analysis of fish tail beat kinematics with simultaneous aerobic and anaerobic measurements to
139 compute energy expended *per tail beat (beat^{-1})*, and compared values for fish in schools to those
140 for solitary fish. Schooling fish reduced TEE•beat^{-1} by 44–126% at higher speeds compared to
141 solitary fish, a substantial reduction in TEE•beat^{-1} consumed both by the school, and by fish in a
142 school (Fig. 3A). Notably, the energetic benefits during active directional schooling occur when
143 fish schools become more streamlined as school length increased with speed and plateaued
144 beyond 2 BL s^{-1} (Fig. 3F), while the three-dimensional distance among individuals stayed
145 relatively constant at ~1.2 BL (Fig 3G). These results directly demonstrate schooling dynamics

146 benefits the swimming kinematics of individual fish and results in a net outcome of up to 112%
147 TEE reduction in fish schools compared to solitary fish.

148 Although the benefits of reducing the energetic cost of locomotion is likely not a major
149 factor underlying the behaviours of low-speed milling[18] and aggregation[19] in fishes, energy
150 conservation is critical for active directional swimming occurring at speeds above 3 BL s^{-1} that
151 are particularly important for evolutionary fitness, *e.g.*, fish swimming in predator-avoidance bait
152 balls[20], during an escape from predators, and food searching group motion[21]. In nature, fish
153 routinely exhibit active directional group locomotion above ~6 BL s^{-1}(Fig. S4, Table S3)[22], a
154 speed that engages anaerobic metabolism. Yet no previous measurement of the anaerobic costs
155 of schooling energetics is available and only one direct measurement of aerobic swimming cost
156 has been reported for a group of four eels[23] at low (aerobic) speeds. Hence, one of the
157 unrecognized but key benefits of active directional group swimming is increased aerobic
158 performance, a reduced need for aerobic capacity and anaerobic energy, and a resultant faster
159 recovery from the associated metabolic perturbations and costs.

160 Quantifying the energetic cost of movement over a wide speed range is directly relevant
161 to understanding fish migratory speeds. The energy use of fish schools shows a *U*-shaped curve
162 (< 3 BL s^{-1}) where swimming at ~1.0 BL s^{-1} consumes less energy than at slower speeds while
163 swimming at 3 BL s^{-1} consumes a similar amount of energy to movement at 0.3 BL s^{-1} (Fig. 1D).
164 Although *Devario aequipinnatus* is not a migratory species, this species does exhibit active
165 directional schooling behaviour and has been a model species for analyses of fish schooling
166 behaviour. These results demonstrate that fish moving in schools can collectively manifest a
167 minimal absolute energetic cost at a mean group swimming speed of ~1.0 BL s^{-1}. Indeed, long-
168 distance swimming commonly occurs in the speed range of 0.5 to 1.5 BL s^{-1} as recorded by tags
169 on migrating fish[2] (Fig. S4; Tables S1, S3,).

The substantial energy conservation resulting from schooling dynamics is critical to understanding rapid collective movement in animals. Fish schooling in a viscous fluid, such as water where drag forces are high, serves as a model for understanding how group movement by animals can be a more energy-efficient biological system than movement by isolated individuals. Individuals in groups gain hydrodynamic benefits to achieving energy conservation, especially when moving at high speeds where there is a premium on energy savings. When a lower proportion of metabolic capacity is devoted to locomotion, animals can apportion more energy to other fitness-related activities, such as digestion, growth and reproduction. More broadly, understanding how collective dynamics of animal movements in the water, land, and air can modify the energy use profiles of individuals will allow us to better understand the ecological, evolutionary and robotic implications of group locomotion.

Methods

Experimental animals

The experiments were performed on giant danio (*Devario aequipinnatus*) that were acquired from a local commercial supplier near Boston, Massachusetts USA (Table S4). Five schooling groups are randomly distributed and housed separately in five 37.9 l aquaria (n=8 per tank). The five solitary individuals are housed separately in five 9.5 l aquaria (n=1 per tank). All aquaria have self-contained thermal control (28 °C), an aeration system (>95 % air saturation, % sat.) and a filtration system. Water changes (up to 50% exchange ratio) were carried out weekly. Fish were fed *ad libitum* daily (TetraMin, Germany). Animal holding and experimental procedures were approved by the Harvard Animal Care IACUC Committee (protocol number 20-03-3).

193 **Integrated Biomechanics & Bioenergetic Assessment Platform (IBBAP)**

194 The core of our experimental system is a 9.35-l (respirometry volume plus tubing)
195 customized Loligo® swim-tunnel respirometer (Tjele, Denmark). The respirometer has an
196 electric motor, and a sealed shaft attached to a propeller located inside the respirometer. By
197 regulating the revolutions per minute (RPM) of the motor, the water velocity of the motor can be
198 controlled. The linear regression equation between RPM and water velocity (V) is established (V
199 = 0.06169*RPM – 5.128, $R^2 = 0.9988$, $p < 0.0001$) by velocity field measured by particle image
200 velocimetry (PIV).

201 The swim-tunnel respirometer is oval-shaped. The central hollow space of the respirometry
202 increases the turning radius of the water current. As a result, the water velocity passing the cross-
203 section of the swimming section (80 × 80 × 225 mm) is more homogenous (validated by PIV).
204 Moreover, a honeycomb flow straightener (80 × 80 × 145 mm) is installed in the upstream of the
205 swimming section to create laminar flow (validated by PIV).

206 To increase the signal-to-noise ratio for the measurement of water dissolved O_2, a water
207 homogenous loop is installed 95 cm downstream of the propeller and the water is returned to the
208 respirometer 240 cm before the swimming section. The flow in the water homogenous loop
209 moves (designated in-line circulation pump, Universal 600, EHEIM GmbH & Co KG, Deizisau,
210 Germany) in the same direction as the water flow in the swimming tunnel. A high-resolution
211 fibre optic O_2 probe (Robust oxygen probe OXROB2, PyroScience GmbH, Aachen, Germany) is
212 sealed in the homogenous loop at the downstream of the circulation pump (better mixing) to
213 continuously measure the dissolved O_2 level in the water (recording frequency ~1 Hz, response
214 time < 15s). The oxygen probe was calibrated to anoxic (0 % sat., a solution created by super-
215 saturated sodium sulphite and bubbling nitrogen gas) and fully aerated water (100 % sat.). The
216 background $\dot{M}O_2$ in the swim-tunnel respirometer was measured for 20 min before and after each

217 trial. The average background $\dot{M}O_2$ (< 6% of fish $\dot{M}O_2$) was used to correct for the $\dot{M}O_2$ of fish.
218 The pre-filtered water (laboratory grade filtration system) is constantly disinfected by UV light
219 (JUP-01, SunSun, China) located in an external water reservoir to suppress the growth of
220 microbials. Water changes of 60% total volume occurred every other day and a complete
221 disinfection by sodium hypochlorite is conducted weekly (Performance bleach, Clorox & 1000
222 ppm).

223 To simultaneously measure schooling dynamics and swimming kinematics, the customized
224 oval-shaped swim-tunnel respirometer is located on a platform with an open window beneath the
225 swimming section. The platform is elevated 243 mm above the base to allow a front surface
226 mirror to be installed at a 45° angle. This mirror allows a high-speed camera (FASTCAM Mini
227 AX50 type 170K-M-16GB, Phontron Inc., United States, lens: Nikon 50mm F1.2, Japan) to
228 record the ventral view. The second camera (FASTCAM Mini AX50 type 170K-M-16GB,
229 Phontron Inc., United States, lens: Nikon 50mm F1.2, Japan) is positioned 515 mm to the side of
230 the swimming section to record a lateral view. Synchronized lateral and ventral video recordings
231 were made at 125 fps, and each frame was 1024 by 1024 pixels. To avoid light refraction passing
232 through the water and distorting the video recordings, the swim-tunnel respirometry is not
233 submerged in the water bath. Temperature regulation of the respirometer is achieved by
234 regulating room temperature, installing thermal insulation layers on the respirometry and
235 replenishing the water inside the respirometer from a thermally regulated (28 °C, heater: ETH
236 300, Hydor, United States & chiller: AL-160, Baoshishan, China) water reservoir (insulated
237 37.9-l aquarium) located externally.

238 The aerated (100% sat., air pump: whisper AP 300, Tetra, China) reservoir water is flushed
239 (pump: Universal 2400, EHEIM GmbH & Co KG, Deizisau, Germany) to the respirometer
240 through an in-line computer-controlled motorized ball valve (U.S. Solid) installed at the in-flow

241 tube. The other in-line one-way valve is installed at the out-flow tube. The out-flow tube is also
242 equipped with a valve. The value is shut during the measurement period, a precautionary practice
243 to eliminate the exchange of water between the respirometer and the external reservoir when the
244 water moves at a high velocity inside the respirometer. This flushing was manually controlled to
245 maintain DO above 80 % sat. Every time the respirometer was closed to measure $\dot{M}O_2$, the water
246 temperature fluctuates no more than 0.2 °C. The water temperature inside the respirometer is
247 measured by a needle temperature probe (Shielded dipping probe, PyroScience GmbH, Aachen,
248 Germany) sealed through a tight rubber port of the respirometer.

249 To allow fish to reach the undisturbed quiescent state during the trial, the entire Integrated
250 Integrated Biomechanics & Bioenergetic Assessment Platform (IBBAP) is covered by laser
251 blackout sheet (Nylon Fabric with Polyurethane Coating; Thorlabs Inc, New Jersey, United
252 States). The room lights are shut off and foot traffic around the experimental rig is restrained to
253 the absolute minimum. Fish are orientated by dual small anterior spots of white light (lowest
254 light intensity, Model 1177, Cambridge Instruments Inc, New York, United States) for
255 orientation (one to the top and the other to the side) of the swimming section. The test section is
256 illuminated by infrared light arrays.

257

258 **Experimental Protocol**

259 We studied five replicate schools and five replicate individuals drawn from within each
260 school. Swimming performance test trials were conducted with *Devario aequipinnatus* fasted for
261 24 hours, a sufficient period for a small species at 28 °C (*i.e.* high resting $\dot{M}O_2$) to reach an
262 absorptive state. In fact, we observed no specific dynamic action, the amount of oxygen
263 consumed for digestion during the first diurnal cycle (Fig. S3). Prior to the swimming
264 performance test, testing fish were gently weighted and placed in the swim-tunnel respirometer.

265 The fish swam at 35% U_{crit} for 30 mins to help oxidize the inevitable but minor lactate
266 accumulation during the prior handling and help fish become accustomed to the flow conditions
267 in the swim-tunnel respirometer [24]. After this time, the fish to be tested were habituated (>20
268 hours) to the respirometer environment under quiescent and undisturbed conditions. During this
269 time, we used an automatic system to measure the resting $\dot{M}O_2$ for at least 19 hours. Relays
270 (Cleware GmbH, Schleswig, Germany) and software (AquaResp v.3, Denmark) were used to
271 control the intermittent flushing of the respirometer with fresh water throughout the trial to
272 ensure O_2 saturation of the respirometer water. $\dot{M}O_2$ was calculated from the continuously
273 recorded dissolved O_2 level (at 1 Hz) inside the respirometer chamber. The intermittent flow of
274 water into the respirometer occurred over 930 s cycles with 30 s where water was flushed into
275 the respirometer and 900 s where the pumps were off and the respirometer was a closed system.
276 The first 240 s after each time the flushing pump was turned off were not used to measure $\dot{M}O_2$
277 to allow O_2 levels inside the respirometer to stabilize. The remaining 660 s when the pumps were
278 off during the cycle were used to measure $\dot{M}O_2$. The in-line circulation pump for water in the O_2
279 measurement loop stayed on throughout the trial.

280 We characterize the swimming performance of fish using an established incremental step-
281 wise critical swimming speed (U_{crit}) test[10]. The first preliminary trial determined the U_{crit} of this
282 population of *Devario aequipinnatus* as 8 BL s^{-1}. Characterizing the swimming performance
283 curve required a second preliminary trial to strategically select 10 water velocities (0.3, 0.5, 0.8,
284 1.0, 1.3, 1.5, 1.8, 2.3, 2.8 BL s^{-1}) to bracket the hypothesized *U*-shaped metabolism-speed curve
285 at the lower speed (< 40% U_{crit}). Additional five water velocities (3.8, 4.9, 5.9, 6.9, 8.0 BL s^{-1})
286 are used to characterize the exponentially increasing curve to the maximum and sustained
287 swimming speed, U_{crit} (*see* Fig. S5). Altogether, 14 points provide a reliable resolution to
288 characterize the swimming performance curve. At each water velocity, fish swam for 10 mins[25]

289 to reach a steady state in $\dot{M}O_2$ at low speeds (*see* Fig. S6). Above 40% U_{crit}, $\dot{M}O_2$ can become
290 more variable[26]. Hence, in this protocol, we focus on measuring the sustained aerobic energy
291 expenditure by calculating the average $\dot{M}O_2$ for each 10-min velocity step using Eqn 1. The
292 respirometry system reaches a stable signal-to-noise ratio once the sampling window is longer
293 than 1.67 mins (*see* Fig. S7), well within the duration of the velocity step to obtain a stable
294 signal-to-noise ratio for calculating $\dot{M}O_2$[26]. At the 5th min of each velocity step, both ventral and
295 lateral-view cameras are triggered simultaneously to record 10-sec footage at 125 frames per
296 second, at 1/1000 shutter speed and 1024 ×1024 pixel resolution. Thus, both data streams of
297 $\dot{M}O_2$ and high-speed videos are recorded simultaneously. The U_{crit} test is terminated when 12.5%
298 of fish in the school or a solitary individual touches the back grid of the swimming section for
299 more than 20 secs[24]. The U_{crit} test lasted ~140 mins and estimates the aerobic portion of energy
300 expenditure over the entire range of swimming performance.

301 To measure the contribution of non-aerobic O_2 cost, where the majority of the cost is related
302 to substrate-level phosphorylation, and to calculate the total energy expenditure for swimming
303 over the entire speed range, we measured excess post-exercise oxygen consumption (EPOC)
304 after the U_{crit} test for the ensuing 19 hours, recorded by an automatic system. Most previous
305 measurements of EPOC have used a duration of ~5 hours, but our extended measurement period
306 ensured that longer duration recovery O_2 consumption during EPOC was measured completely
307 as fish were exercised to U_{crit} (*see* summary table in *16*). The intermittent flow of water into the
308 respirometer occurred over 30 s to replenish the dissolved O_2 level to ~95% sat. For the
309 following 900 s the flushing pump remained closed, and the respirometer becomes a closed
310 system, with the first 240 s to allow O_2 saturation inside the respirometer to stabilize. The
311 remaining 660 s when the flushing pump was off during the cycle were used to measure $\dot{M}O_2$
312 (*see* Eqn 1). The cycle is automated by computer software (AquaResp v.3) and provided 74

measurements of $\dot{M}O_2$ to compute EPOC. Upon the completion of the three-day protocol, the school or individual fish are returned to the home aquarium for recovery. The fish condition was closely monitored during the first 48 hours after the experiment, during which no mortality was observed.

Bioenergetic measurement and modeling

To estimate the steady-rate whole-animal aerobic metabolic rate, $\dot{M}O_2$ values were calculated from the sequential interval regression algorithm (Eqn. 1) using the dissolved O_2 (DO) points continuously sampled (~1 Hz) from the respirometer.

$$\dot{\mathrm{M}}\mathrm{O}_2 = \left[\frac{d_{DO_{[i,(i+a)]}}}{d_{t_{[i,(i+a)]}}} * \left(V_r - V_f\right) * S_O\right] / (t * M_f) \text{(Eqn. 1)}$$

Where d_{DO}/d_t is the change in O_2 saturation with time, V_r is the respirometer volume, V_f is the fish volume (1 g body mass = 1 ml water), S_o is the water solubility of O_2 (calculated by AquaResp v.3 software) at the experimental temperature, salinity and atmospheric pressure, t is a time constant of 3600 s h^{-1}, M_f is fish mass, and a is the sampling window duration, i is the next PO_2 sample after the preceding sampling window.

To account for allometric scaling, the $\dot{M}O_2$ values of solitary fish were transformed to match the size of the individual fish in the school (*see* Table S4) using an allometric scaling exponent (b = 0.7546). The calculation of scaling relationship [$\mathrm{Log}_{10}(\dot{M}O_2) = b \bullet \mathrm{Log10}(M) + \mathrm{Log10}(a)$, where M is the body mass & a is a constant] were performed by least squares linear regression analysis ($y = 0.7546*x + 0.2046$; $R^2 = 0.6727$, $p < 0.0001$) on the 180 data points of metabolic rate and body mass from a closely related species (the best available dataset to our knowledge)[28]. The allometrically scaled $\dot{M}O_2$ values were used to derive other energetic metrics (listed below)

for the solitary fish. The energetic metrics of fish schools are calculated from the mass-specific $\dot{M}O_2$.

The resting oxygen uptake ($\dot{M}O_{2rest}$), the minimum resting metabolic demands of a group of fish or a solitary individual, is calculated from a quantile 20% algorithm[29] using the $\dot{M}O_2$ estimated between the 10th–18th hour and beyond the 32nd hour of the trial. These are the periods of quiescent state when fish completed the EPOC from handling and swimming test.

The $\dot{M}O_2$ for the aggregation (Fig. 1B, $\dot{M}O_{2aggregate}$) is calculated as the average value using the $\dot{M}O_2$ estimated between the 10th–18th hour without the effects of any tests.

Minimum oxygen uptake ($\dot{M}O_{2min}$) is the lowest $\dot{M}O_2$ value recorded in the entire trial, which always occurred at the optimal speed when a school of fish collectively reached the lowest $\dot{M}O_2$ value.

Active oxygen uptake ($\dot{M}O_{2active}$) is the highest average $\dot{M}O_2$ when fish are actively swimming[10].

The aerobic scope is the numerical difference between $\dot{M}O_{2active}$ and $\dot{M}O_{2min}$ (*i.e.* $\dot{M}O_{2active} - \dot{M}O_{2min}$)[10].

The percentage of aerobic scope (% aerobic scope) is calculated by normalizing the $\dot{M}O_2$ value at a water velocity as a % aerobic scope [($\dot{M}O_2 - \dot{M}O_{2min}$) / ($\dot{M}O_{2active} - \dot{M}O_{2min}$)]. The apportioning of aerobic scope to swimming performance is computed across the entire range of swim speeds.

The excess post-exercise oxygen consumption (EPOC) is an integral area of $\dot{M}O_2$ measured during post-exercise recovery, from the end of U_{crit} until reached $\dot{M}O_{2rest}$ plus 10%[27]. This approach reduces the likelihood of overestimating EPOC due to spontaneous activities[27]. To account for the allometric scaling effect, we used the total amount of O_2 consumed (mg O_2) by the standardized body mass of fish (1.66 g) for fish schools and solitary fish.

360 We model EPOC (*i.e.* non-aerobic O_2 cost) to estimate a *total* O_2 cost over the duration of
361 the swimming performance test. Our conceptual approach was pioneered by Brett[10] in fish and is
362 also used in sports science[9]. Mathematical modeling was applied to study the effects of
363 temperature on the cost of swimming for migratory salmon[24]. We improved the mathematical
364 modeling by applying the following physiological and physics criteria. The first criterion is that
365 significant accumulation of glycolytic end-product occurred when fish swimming above 50%
366 U_{crit}[16] which corresponds to > 40% $\dot{M}O_{2max}$ (or ~ 50% aerobic scope)[9]. This is also when fish
367 start unsteady-state burst-&-glide swimming gait[16]. The second criterion is that the integral area
368 for the non-aerobic O_2 cost during swimming can only differ by ≤ 0.09% when compared to
369 EPOC. The non-aerobic O_2 cost during swimming is the area bounded by modeled $\dot{M}O_2$ and
370 measured $\dot{M}O_2$ as a function of time when fish swim > 50% U_{crit} (*see* Fig. 2A & Table S2). The
371 third criterion is that total energy expenditure is expected to increase exponentially with
372 swimming speed (Fig. S8). Specifically, these curves were fitted by power series or polynomial
373 models, the same models that describe the relationship between water velocity and total power
374 and energy cost of transport (Fig. S8). Following these criteria, the non-aerobic O_2 cost at each
375 swimming speed is computed by a percentage (%) modifier based on the aerobic O_2 cost (Table
376 S2). The exponential curve of total O_2 cost as swimming speed of each fish school or solitary
377 individual was derived by an iterative process until the difference between non-aerobic O_2 cost
378 and EPOC met the 2nd criterion. The sum of non-aerobic O_2 cost and aerobic cost gives the total
379 O_2 cost.

380 Total energy expenditure (TEE) is calculated by converting total O_2 cost to kJ × kg^{-1} using
381 an oxy-calorific equivalent of 3.25 cal per 1 mg O_2 [30].

382 Cost of transport (COT), in kJ × km^{-1} × kg^{-1} is calculated by dividing TEE by speed (in km
383 × h^{-1})[25].

384

385 **Three-dimensional kinematic data extraction from high-speed videography**

386 We used two synchronized 10-sec high-speed videos (lateral and ventral views, at each
387 speed) for kinematic analyses. We calibrated the field of view of the high-speed cameras using a
388 direct linear transformation for three-dimensional kinematic reconstruction (DLTdv8)[31] by
389 applying a stereo calibration to the swimming section of the respirometer (*see* Fig. S9). We
390 digitized the anatomical landmarks of fish (*see* Fig. S10) to obtain the X, Y, Z coordinates for
391 each marker at the 1st sec, 5th sec and 10th sec for videos recorded at each speed. These
392 coordinates are used to calculate the following kinematic parameters. All the calculations are
393 validated on the known length and angle of test objects inserted into the tank working section.

394 The three-dimensional distance between the tip of the nose of each fish in the school per
395 frame is calculated in vector Eqn. 2

396 $$d = \sqrt{(Xa - Xb)^2 + (Ya - Yb)^2 + (Za - Zb)^2} \quad \text{(Eqn. 2)}$$

397 Where spatial coordinates of two neighbouring fish are (X_a, Y_a, Z_a) and (X_b, Y_b, Z_b)
398 respectively.

399 The three-dimensional angle of each fish in the school to the frontal plane per frame is
400 calculated by Eqn. 3

401 $$\theta = \arccos \frac{(X2-X1)\cdot(X3-X1)+(Y2-Y1)\cdot(Y3-Y1)+(Z2-Z1)\cdot(Z3-Z1)}{\sqrt{(X2-X1)^2\cdot(Y2-Y1)^2\cdot(Z2-Z1)^2}\cdot\sqrt{(X3-X1)^2\cdot(Y3-Y1)^2\cdot(Z3-Z1)^2}} \quad \text{(Eqn. 3)}$$

402 where the spatial coordinates of the caudal peduncle, nose of fish and right angle crosshair
403 between the peduncle and the nose are (X_1, Y_1, Z_1), (X_3, Y_3, Z_3) and (X_2, Y_2, Z_2) respectively (*see*
404 Fig. S10).

405 The fish's angle to water flow per frame is calculated using the arctangent function in Excel
406 (Microsoft, United States) using the spatial coordinates of the caudal peduncle and nose of the
407 fish.

408 The school length (in *X* axis) is calculated as a three-dimensional distance (Eqn. 2) between
409 the nose of the first fish of the school to the caudal peduncle of the last fish in the school.

410 Tail beat frequency (TBF), in Hz, is calculated as the number of tail beats observed within
411 one second. We sampled 10 tail beats from fish exhibiting steady-state swimming to obtain an
412 average and representative TBF for each solitary fish at each speed. We sampled 10 tail beats of
413 steady-state swimming for three individuals in the center of the fish school for an average and
414 representative TBF for each fish school.

415 The values calculated above were averaged among the three frames at each speed as a
416 representative kinematic feature of the schools (or solitary fish) for each speed. The standard
417 deviation of the angle to water flow in fish schools is calculated from the angular values of the
418 individuals.

419 Turning frequency is the total number of events when fish made a 90˚ turn in the 10-sec
420 video. To make the total number of turns per individual and fish schools comparable (multiple
421 individuals inevitably have a larger absolute number of turns), we derived the average turning
422 frequency per schooling fish by dividing the total number of turns of fish school by the number
423 of fish in the school.

424 Stride length (BL) is calculated as the relative swimming speed (BL s^{-1}) of a fish over one
425 cycle of the tail beat ($U \bullet TBF^{-1}$)[32].

426 Total energy expenditure per tail beat (kJ kg^{-1} $beat^{-1}$) is calculated by $TEE \bullet TBF^{-1}$ to estimate
427 the total metabolic energy spent to achieve one stride length. Additional calculations done were:

Strouhal number = (TBF • tail beat amplitude) • U^{-1} [5]. Tail beat amplitude is measured as the average distance of five peak-to-peak oscillation amplitudes of the tip of the fish's tail. The measurement is conducted on the calibrated high-speed video in video analysis software (Phontron FASTCAM Viewer 4, Photron USA, Inc.).

Reynolds number = (water density • U • fish fork length) • water dynamic viscosity $^{-1}$ [5]. Water density and dynamic viscosity are given at 28 °C.

Statistical analyses

Measurement points are presented as mean ± s.e.m. For the metrics that failed normality tests, logarithm transformations were applied to meet the assumptions of normality of residuals, homoscedasticity of the residuals, and no trend in the explanatory variables. The majority of statistical comparisons used two-way (solitary fish vs. fish schools & swimming speed) ANOVA with Holm–Šídák *post-hoc* tests. The few comparisons that used other statistical models are listed below. The comparison of $\dot{M}O_{2min}$ at optimal speed, $\dot{M}O_2$ of aggregating behaviours exhibited at the lowest speed ($\dot{M}O_{2aggregate}$) and resting $\dot{M}O_2$ ($\dot{M}O_{2rest}$) in fish schools used one-way ANOVA with Holm–Šídák *post-hoc* tests. The comparison of EPOC between solitary fish and fish schools used a two-tailed Student's t-test. The comparison of the duration of EPOC between solitary fish and fish schools used a two-tailed Student's t-test. The overall difference in percentage aerobic scope (% aerobic scope) between fish schools and solitary individuals is compared by the Wilcoxon singed-rank test over the entire range of 14 swimming speeds. The statistical analyses were conducted in SPSS v.28 (SPSS Inc. Chicago, IL, USA). The best-fitting regression analyses were conducted using Prism v.9.4.1 (GraphPad Software, San Diego, CA, USA). 95% C.I. values were presented for all regression models as shaded areas around the

regression or data points. Statistical significance is denoted by *, **, ***, **** for *p*-values of ≤ 0.05, ≤ 0.01, ≤ 0.001, ≤ 0.0001 respectively.

References and Notes

1. Weihs, D. Hydromechanics of fish schooling. *Nature* **241**, 290–291 (1973).
2. Block, B. A. *et al.* Electronic tagging and population structure of Atlantic bluefin tuna. *Nature* **434**, 1121–1127 (2005).
3. Block, B. A., Booth, D. & Carey, F. G. Direct measurement of swimming speeds and depth of blue marlin. *Journal of Experimental Biology* **166**, 267–284 (1992).
4. Biewener, A. & Patek, S. *Animal Locomotion*. (Oxford University Press, 2018).
5. Vogel, S. *Life in Moving Fluids: The Physical Biology of Flow - Revised and Expanded Second Edition*. (Princeton University Press, 2020).
6. Weimerskirch, H., Martin, J., Clerquin, Y., Alexandre, P. & Jiraskova, S. Energy saving in flight formation. *Nature* **413**, 697–698 (2001).
7. Blocken, B. *et al.* Aerodynamic drag in cycling pelotons: New insights by CFD simulation and wind tunnel testing. *Journal of Wind Engineering and Industrial Aerodynamics* **179**, 319–337 (2018).
8. Shinichiro, I. Aerodynamic effects by marathon pacemakers on a main runner. *Transactions of the Japan Society of Mechanical Engineers Part B* **73**, 1975–1980 (2007).
9. Laforgia, J., Withers, R. T. & Gore, C. J. Effects of exercise intensity and duration on the excess post-exercise oxygen consumption. *Journal of Sports Sciences* **24**, 1247–1264 (2006).
10. Brett, J. R. The Respiratory Metabolism and Swimming Performance of Young Sockeye Salmon. *J. Fish. Res. Bd. Can.* **21**, 1183–1226 (1964).

11. Li, L. *et al.* Vortex phase matching as a strategy for schooling in robots and in fish. *Nat Commun* **11**, 5408 (2020).
12. Jones, K. D., Dohring, C. M. & Platzer, M. F. Experimental and computational investigation of the Knoller-Betz effect. *AIAA Journal* **36**, 1240–1246 (1998).
13. Gaesser, G. A. & Brooks, G. A. Metabolic bases of excess post-exercise oxygen consumption: a review. *Med Sci Sports Exerc* **16**, 29–43 (1984).
14. Jayne, B. C. & Lauder, G. V. New data on axial locomotion in fishes: How speed affects diversity of kinematics and motor patterns. *American Zoologist* **36**, 642–655 (1996).
15. Rome, L. C., Loughna, P. T. & Goldspink, G. Temperature acclimation: Improved sustained swimming performance in carp at low temperatures. *Science* **228**, 194–196 (1985).
16. Peake, S. J. & Farrell, A. P. Postexercise physiology and repeat performance behaviour of free-swimming smallmouth bass in an experimental raceway. *Physiological and Biochemical Zoology* **78**, 801–807 (2005).
17. Xu, N. W. & Dabiri, J. O. Low-power microelectronics embedded in live jellyfish enhance propulsion. *Science Advances* **6**, eaaz3194 (2020).
18. Costanzo, A. & Hemelrijk, C. K. Spontaneous emergence of milling (vortex state) in a Vicsek-like model. *J. Phys. D: Appl. Phys.* **51**, 134004 (2018).
19. Rountree, R. A. Association of fishes with fish aggregation devices: Effects of structure size on fish abundance. *Bulletin of Marine Science* **44**, 960–972 (1989).
20. Stewart, J. D., Barroso, A., Butler, R. H. & Munns, R. J. Caught at the surface: myctophids make easy prey for dolphins and devil rays. *Ecology* **99**, 1894–1896 (2018).
21. Pitcher, T. J., Magurran, A. E. & Winfield, I. J. Fish in larger shoals find food faster. *Behav Ecol Sociobiol* **10**, 149–151 (1982).

22. Misund, O. A. & Aglen, A. Swimming behaviour of fish schools in the North Sea during acoustic surveying and pelagic trawl sampling. *ICES Journal of Marine Science* **49**, 325–334 (1992).

23. Burgerhout, E. *et al.* Schooling reduces energy consumption in swimming male European eels, Anguilla anguilla L. *Journal of Experimental Marine Biology and Ecology* **448**, 66–71 (2013).

24. Lee, C. G., Farrell, A. P., Lotto, A., Hinch, S. G. & Healey, M. C. Excess post-exercise oxygen consumption in adult sockeye (*Oncorhynchus nerka*) and coho (*O. kisutch*) salmon following critical speed swimming. *Journal of Experimental Biology* **206**, 3253–3260 (2003).

25. Di Santo, V., Kenaley, C. P. & Lauder, G. V. High postural costs and anaerobic metabolism during swimming support the hypothesis of a U-shaped metabolism–speed curve in fishes. *Proceedings of the National Academy of Sciences* **114**, 13048–13053 (2017).

26. Zhang, Y., Gilbert, M. J. H. & Farrell, A. P. Finding the peak of dynamic oxygen uptake during fatiguing exercise in fish. *Journal of Experimental Biology* **222**, (2019).

27. Zhang, Y., Claireaux, G., Takle, H., Jørgensen, S. M. & Farrell, A. P. A three-phase excess post-exercise oxygen consumption in Atlantic salmon *Salmo salar* and its response to exercise training. *J Fish Biol* **92**, 1385–1403 (2018).

28. Wootton, H. F., Morrongiello, J. R., Schmitt, T. & Audzijonyte, A. Smaller adult fish size in warmer water is not explained by elevated metabolism. *Ecology Letters* **25**, 1177–1188 (2022).

29. Chabot, D., Steffensen, J. F. & Farrell, A. P. The determination of standard metabolic rate in fishes. *Journal of Fish Biology* **88**, 81–121 (2016).

30. Brafield, A. E. & Solomon, D. J. Oxy-calorific coefficients for animals respiring nitrogenous substrates. *Comparative Biochemistry and Physiology Part A: Physiology* **43**, 837–841 (1972).

31. Hedrick, T. L. Software techniques for two- and three-dimensional kinematic measurements of biological and biomimetic systems. *Bioinspir. Biomim.* **3**, 034001 (2008).

32. Bainbridge, R. The speed of swimming of fish as related to size and to the frequency and amplitude of the tail beat. *Journal of Experimental Biology* **35**, 109–133 (1958).

Acknowledgments: Many thanks to members of Lauder Laboratory for numerous discussions about fish schooling behaviour, for comments on the manuscript, and to Cory Hahn for fish care.

Funding: Funding provided by the National Science Foundation grant 1830881 (GVL), the Office of Naval Research grants N00014-21-1-2661 (GVL), N00014-16-1-2515 (GVL), 00014-22-1-2616 (GVL), and a Postdoctoral Fellowship of Natural Sciences and Engineering Research Council of Canada PDF - 557785 – 2021 (YZ).

Author contributions:

Y.Z. and G.L. conceptualized the study. Y.Z. performed experiments and data analyses and wrote the manuscript. Y.Z. and G.L. provided manuscript edits and comments and approved the final version.

Competing interests: Authors declare that they have no competing interests.

Data and materials availability: All data generated or analysed during this study are included in this published article (and its supplementary information files).

Supplementary Materials:
Introductory text
Figs. S1 to S10
Tables S1 to S4
Captions for Movies S1 to S3

Other Supplementary Materials for this manuscript include the following:

Movies S1 to S3

FIGURES & FIGURE CAPTIONS

555

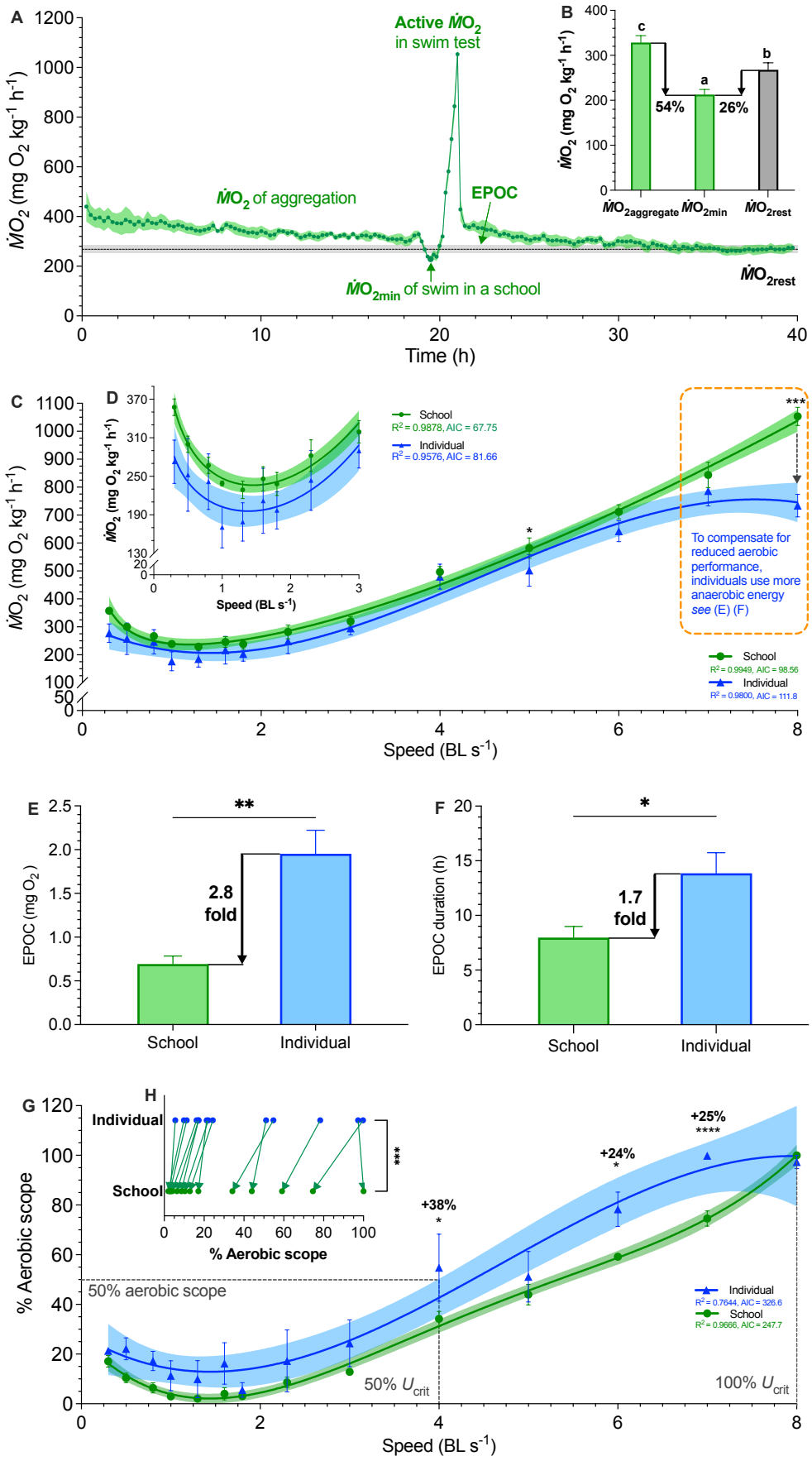
A
Active $\dot{M}O_2$ in swim test
$\dot{M}O_2$ of aggregation
EPOC
$\dot{M}O_{2min}$ of swim in a school
$\dot{M}O_{2rest}$
$\dot{M}O_2$ (mg O_2 kg^{-1} h^{-1})
Time (h)
B
54%
26%
$\dot{M}O_{2aggregate}$
$\dot{M}O_{2min}$
$\dot{M}O_{2rest}$
C
D
School
R^2 = 0.9878, AIC = 67.75
Individual
R^2 = 0.9576, AIC = 81.66
Speed (BL s^{-1})
To compensate for reduced aerobic performance, individuals use more anaerobic energy see (E) (F)
School
R^2 = 0.9949, AIC = 98.56
Individual
R^2 = 0.9800, AIC = 111.8
E
EPOC (mg O_2)
2.8 fold
School
Individual
F
EPOC duration (h)
1.7 fold
G
H
Individual
School
% Aerobic scope
+38%
+24%
+25%
50% aerobic scope
50% U_{crit}
100% U_{crit}
Individual
R^2 = 0.7644, AIC = 326.6
School
R^2 = 0.9666, AIC = 247.7

556 **Fig. 1. Measurements of aerobic and anaerobic locomotor cost of fish schools and solitary**
557 **fish.** (**A**) Average traces of metabolic rate ($\dot{M}O_2$) of fish schools over a 40-hour experiment.
558 Following the first 18-h quiescent state, a critical swimming speed (U_{crit}) test quantifies the
559 aerobic cost of active swimming. The ensuing 18-h measurement of excess post-exercise oxygen
560 consumption (EPOC) quantifies the anaerobic cost. (**B**) Comparison of $\dot{M}O_2$ for conditions of
561 aggregating behaviour, minimum demand speed, and resting condition with the minimal flow
562 ($\dot{M}O_{2aggregate}$, $\dot{M}O_{2min}$, $\dot{M}O_{2rest}$) (**C**) Comparisons of *J*-shaped $\dot{M}O_2$-speed curve over the entire
563 range (0.3–8 body length s^{-1}, BL s^{-1}) and (**D**) *U*-shaped $\dot{M}O_2$-speed curve at the lower speeds
564 (0.3–3 BL s^{-1}). (**E**, **F**) Comparisons of EPOC and EPOC durations between fish schools and
565 solitary fish. (**G, H)** Percentage (%) aerobic scope used by fish schools and solitary fish during
566 the U_{crit} test. Statistical significance is denoted by asterisk(s). Green color = school data (n=5);
567 blue color = solitary fish data (n=5); shading indicates the 95% confidence interval. Statistical
568 details are available in the statistical analyses section.

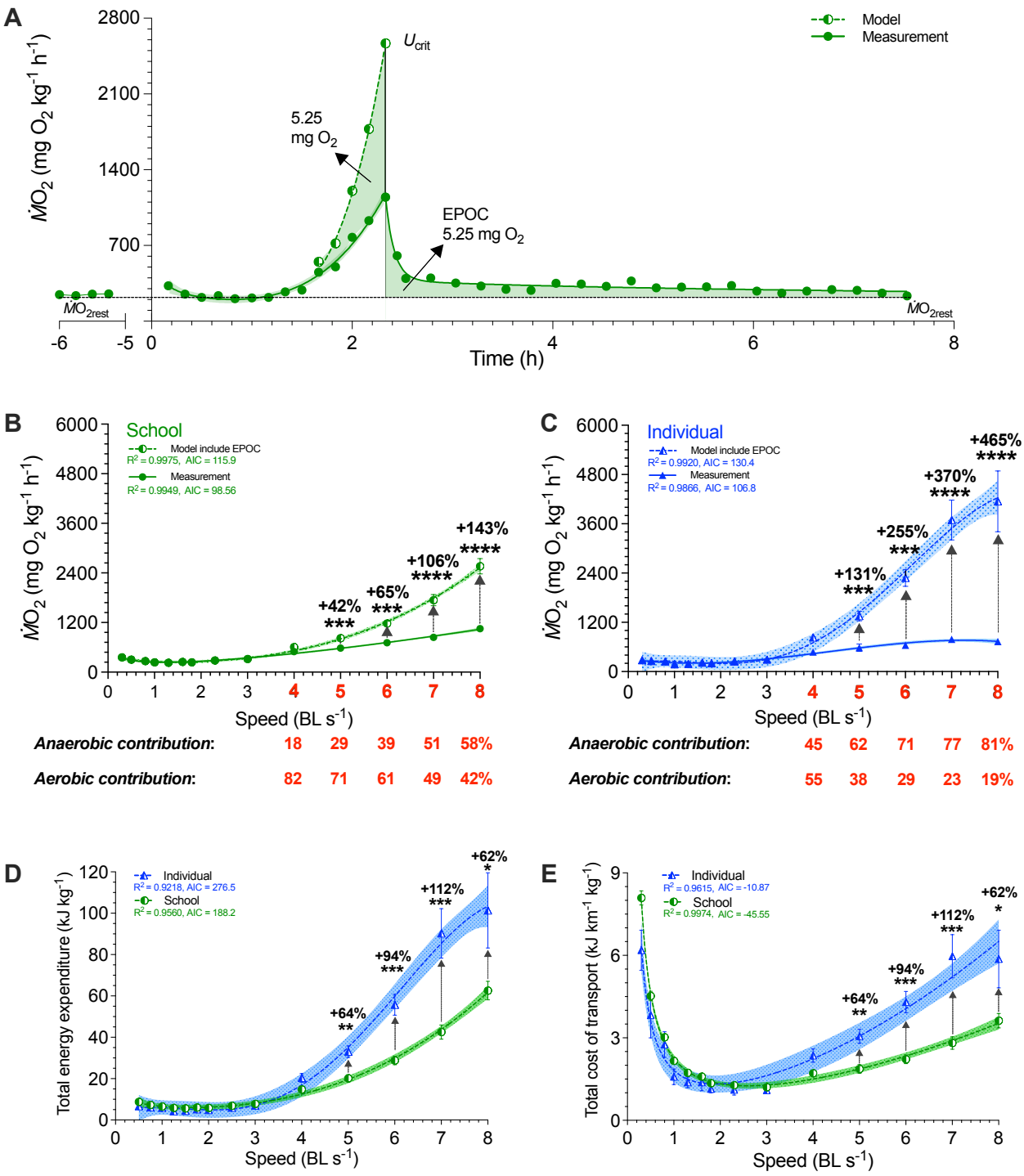
A
Model
Measurement
U_{crit}
5.25 mg O_2
EPOC 5.25 mg O_2
$\dot{M}O_{2rest}$
$\dot{M}O_2$ (mg O_2 kg^{-1} h^{-1})
Time (h)
B
School
Model include EPOC
R^2 = 0.9975, AIC = 115.9
Measurement
R^2 = 0.9949, AIC = 98.56
+42% ***
+65% ***
+106% ****
+143% ****
Speed (BL s^{-1})
Anaerobic contribution: 18 29 39 51 58%
Aerobic contribution: 82 71 61 49 42%
C
Individual
Model include EPOC
R^2 = 0.9920, AIC = 130.4
Measurement
R^2 = 0.9866, AIC = 106.8
+131% ***
+255% ***
+370% ****
+465% ****
Anaerobic contribution: 45 62 71 77 81%
Aerobic contribution: 55 38 29 23 19%
D
Individual
R^2 = 0.9218, AIC = 276.5
School
R^2 = 0.9560, AIC = 188.2
+64% **
+94% ***
+112% ***
+62% *
Total energy expenditure (kJ kg^{-1})
E
Individual
R^2 = 0.9615, AIC = -10.87
School
R^2 = 0.9974, AIC = -45.55
+64% **
+94% ***
+112% ***
+62% *
Total cost of transport (kJ km^{-1} kg^{-1})

569

570 **Fig. 2. Modeling of simultaneous aerobic and anaerobic costs of fish schools and solitary**
571 **fish for a critical swimming speed (U_{crit}) test. (A)** Modeling the O_2 cost of the metabolic rate
572 ($\dot{M}O_2$)-speed curve and the ensuing recovery cost (excess post-exercise oxygen consumption,
573 EPOC) as a function of speed. After U_{crit}, fish returned to the same resting $\dot{M}O_2$ ($\dot{M}O_{2rest}$) as a
574 pre-test. (**B, C**) In addition to $\dot{M}O_2$ (solid line & filled symbols), we modeled the total O_2 cost
575 (dash line & half-filled symbols) for fish schools and solitary fish and when performing the U_{crit}
576 swimming test. The estimated partitioning of aerobic and anaerobic contributions to swimming
577 are denoted (red-&-bold) with respect to speed for 4–8 BL s^{-1} is shown below each graph. (**D, E**)
578 Using total O_2 cost, we computed total energy expenditure and the total cost of transport
579 (including both aerobic and anaerobic metabolism) for both fish schools and solitary fish.
580 Statistical significance is denoted by asterisk(s). Green color = school data (n=5); blue color =
581 solitary fish data (n=5); shading indicates the 95% confidence interval. See methods for
582 modeling and statistical details.

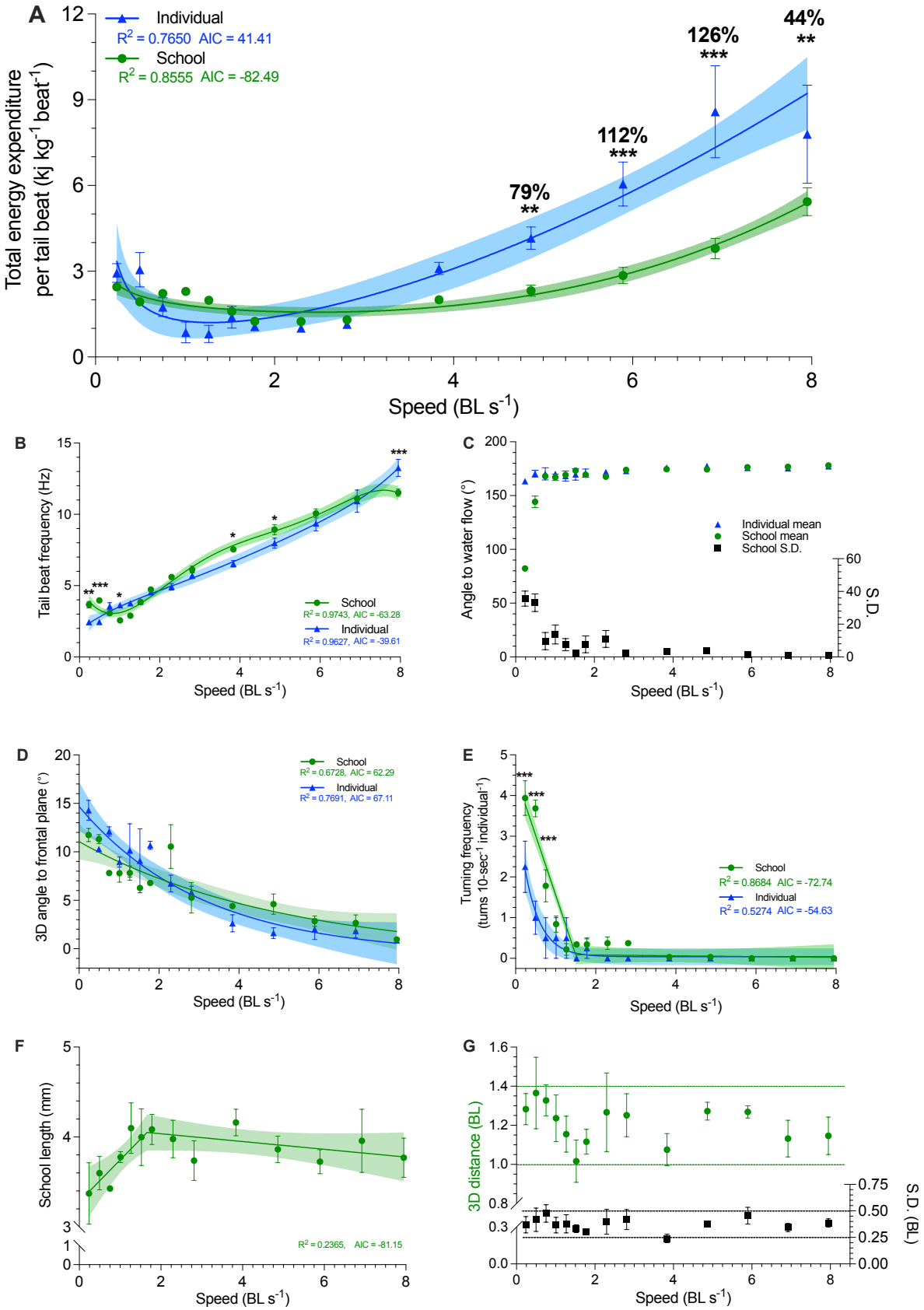
A
Individual
R² = 0.7650 AIC = 41.41
School
R² = 0.8555 AIC = -82.49
Total energy expenditure per tail beat (kj kg⁻¹ beat⁻¹)
Speed (BL s⁻¹)
79% **
112% ***
126% ***
44% **
B
Tail beat frequency (Hz)
School
R² = 0.9743, AIC = -63.28
Individual
R² = 0.9627, AIC = -39.61
C
Angle to water flow (°)
S.D.
Individual mean
School mean
School S.D.
D
3D angle to frontal plane (°)
School
R² = 0.6728, AIC = 62.29
Individual
R² = 0.7691, AIC = 67.11
E
Turning frequency (turns 10-sec⁻¹ individual⁻¹)
School
R² = 0.8684 AIC = -72.74
Individual
R² = 0.5274 AIC = -54.63
F
School length (mm)
R² = 0.2365, AIC = -81.15
G
3D distance (BL)
S.D. (BL)

583

584 **Fig. 3. Three-dimensional characterization of swimming kinematics and fish schooling**
585 **dynamics as a function of speed. (A)** Total energy expenditure per tail beat, (**B**) Tail beat
586 frequency, (**C**) The angle of fish to free-stream water flow, measured as the mean and the S.D. of
587 the angles of the individuals within the school. (**D**) Three-dimensional angle of fish to the frontal
588 plane. (**E**) Turning frequency, (**F**) Three-dimensional school length. (**G**) Three-dimensional
589 distances among all individuals in the school and the S.D. of the distance. The visual illustration
590 of the upper and lower boundaries of the metrics are indicated. Statistical significance is denoted
591 by asterisk(s). Green color = school data (n=3-4); blue color = solitary fish data (n=3-4); shading
592 indicates the 95% confidence interval. See methods for details of three-dimensional
593 reconstruction and statistics.

594

595